PHYSICAL REVIEW B **89**, 245113 (2014)

Effect of isoelectronic doping on the honeycomb-lattice iridate A_2IrO_3

S. Manni,[1] Sungkyun Choi,[2] I. I. Mazin,[3] R. Coldea,[2] Michaela Altmeyer,[4] Harald O. Jeschke,[4] Roser Valentí,[4] and P. Gegenwart[1,*]

[1]*I. Physikalisches Institut, Georg-August-Universität Göttingen, D-37077 Göttingen, Germany*

[2]*Clarendon Laboratory, University of Oxford, Parks Road, Oxford OX1 3PU, United Kingdom*

[3]*Code 6393, Naval Research Laboratory, Washington, DC 20375, USA*

[4]*Institut für Theoretische Physik, Goethe-Universität Frankfurt, D-60438 Frankfurt am Main, Germany*

(Received 3 December 2013; revised manuscript received 7 February 2014; published 11 June 2014)

We have investigated, experimentally and theoretically, the series $(Na_{1-x}Li_x)_2IrO_3$. Contrary to what has been believed so far, only for $x \leqslant 0.25$ does the system form uniform solid solutions where Li preferentially goes to the Ir_2Na planes, as observed in our density functional theory calculations and consistent with x-ray diffraction analysis. For larger Li content, as evidenced by powder x-ray diffraction, scanning electron microscopy, and density functional theory calculations, the system shows a miscibility gap and a phase separation into an ordered $Na_3LiIr_2O_6$ phase with alternating Na_3 and $LiIr_2O_6$ planes, and a Li-rich phase close to pure Li_2IrO_3. For $x \leqslant 0.25$ we observe (1) an increase of c/a with Li doping up to $x = 0.25$, despite the fact that c/a in pure Li_2IrO_3 is smaller than in Na_2IrO_3, and (2) a gradual reduction of the antiferromagnetic ordering temperature T_N and ordered moment. In view of our results showing clear evidence for phase separation for $0.25 \leqslant x \leqslant 0.6$, more detailed studies are needed to confirm the presence or absence of phase separation at the higher doping $x \sim 0.7$, where a continuum quantum phase transition has been proposed previously.

DOI: 10.1103/PhysRevB.89.245113 PACS number(s): 75.40.Cx, 75.10.Jm, 75.40.Gb, 75.50.Lk

I. INTRODUCTION

Quasi-two-dimensional (2D) correlated oxides with honeycomb layers have been attracting considerable interest in the past years [1,2] largely because of their capacity to host interesting topological and frustration phenomena [3,4]. Of particular interest is Na_2IrO_3, where several critical energy scales are comparable, such as one-electron hopping t, Hubbard repulsion U, Hund's rule coupling J, and spin-orbit interaction λ. A possible, albeit not necessary, consequence of the competition between several comparable energy scales is strong frustration, in particular, magnetic, which may lead to long-sought spin-disordered phases at zero temperature.

It was recently proposed [5] that Na_2IrO_3 and Li_2IrO_3 form a continuous solid solution, with the Néel ordering temperature maximized in the end compounds and going nearly to zero at an intermediate doping, $(Na_{1-x}Li_x)_2IrO_3$, $x \sim 0.7$. Such a quantum phase transition would be of great interest, as it would allow going from a quantum spin liquid state to different types of long range order by changing doping in two different directions.

In this paper we show, both experimentally and theoretically, that the assumption of a continuous solid solution is not justified. In particular, for $x > 0.25$, the system experiences a phase separation, which has a profound physical reason. Specifically, we find that the $x = 0.25$ state, namely, the one where all Na in the Ir_2Na planes are substituted by Li while the Na_3 plane remains intact, is exceptionally stable.

This stability is gained through the fact that Li is smaller than Na and therefore allows shorter Ir-Ir bond lengths, when placed in the same plane. Indeed, as was observed earlier [4,6,7], two different Ir-Ir hoppings compete in this system: direct overlap of like orbitals, and indirect, O-assisted hopping of unlike orbitals. Even small changes in geometry dramatically affect this competition. On the other hand, partial substitution of the interlayer Na by Li is not energetically favorable because the interlayer separation is defined by the larger Na ions and is not optimal from the Li point of view. This is why compositions with $x > 0.25$ prefer phase separation.

We also observe a Néel temperature reduction with increasing doping up to $x < 0.25$, as was previously reported [5]. In fact, our findings on the underlying doped lattices are essential to understand both the Néel temperature reductions as pure end members are respectively doped (it is likely that the mechanisms are different for the Na-rich and Li-rich alloys), and the nature of the putative quantum critical point [5]. Most importantly, we observe a chemical phase separated region in the $(Na_{1-x}Li_x)_2IrO_3$ phase diagram for $x > 0.25$ (extending to at least $x = 0.6$), which questions a continuous quantum phase transition (QPT) at $x = 0.7$, as suggested Cao *et al.* [5].

II. EXPERIMENTAL DETAILS

Single crystals of $(Na_{1-x}Li_x)_2IrO_3$ have been grown using a similar procedure as previously used for Na_2IrO_3 [1]. A first calcination process has been done at 750 °C with stoichiometric proportions of carbonates (Na_2CO_3 and Li_2CO_3) and Ir metal. After prereaction at 900 °C, the polycrystalline material was processed for crystal growth with excess IrO_2 flux. The amount of excess IrO_2 and the temperature of crystal growth were varied for different doping levels. Since with increasing Li content the solubility of the phase in the flux decreases, it is important to control both temperature and excess IrO_2 to obtain large enough crystals for bulk measurements.

The Na:Li ratio was determined by inductively coupled plasma mass spectrometry (ICPMS) on different pieces of crystals of every doping level. In contrast to the claim of Ref. [5], we have found that it is not possible to detect Li by an energy dispersive x-ray (EDX) analysis since Li is a light metal. In EDX we can only observe changes in the Na to Ir

*Present address: EP VI, Center for Electronic Correlations and Magnetism, Augsburg University, 86159 Augsburg, Germany.

TABLE I. Comparison between the nominal and actual Li content determined by ICPMS in percent (%) of Li in $(Na_{1-x}Li_x)_2IrO_3$.

x	Nominal Li (%)	ICPMS Li (%)
0.05	5	3.83 (±0.2)
0.1	10	9.5 (±0.5)
0.2	20	21.8 (±1.5)
0.3	30	33.2 (±1.1)
0.4	40	47.0 (±0.9)

ratio, which decreases with Li doping. Table I gives a comparison between the nominal (starting composition) and the measured Li fractions. Some of the platelike crystals were crushed and powder x-ray diffraction (XRD) was performed for the scattering angle range $10^\circ \leqslant 2\theta \leqslant 100^\circ$ with Cu$K\alpha$ radiation to estimate the change of the lattice parameters with Li doping. Single-crystal x-ray diffraction (XRD) was performed using a Mo-source Oxford Diffraction Supernova diffractometer on crystals of $(Na_{1-x}Li_x)_2IrO_3$ with nominal doping x from 0.05 to 0.4 in order to obtain lattice parameters and confirm the crystal structure and internal atomic coordinates. The samples were thin, platelike crystals with a typical size of $70 \times 60 \times 10\ \mu m^3$. Magnetization, ac susceptibility, and specific heat were measured in commercial superconducting quantum interference device (SQUID) magnetometer and physical property measurement systems, respectively.

Since the size of Li-doped crystals decreases with doping, we have used lumps of crystals for magnetization and specific heat measurements. Crystals (or lumps) have been separated mechanically. Sometimes some remaining flux is present in the lump, which gives a low temperature Curie tail in the $\chi(T)$ measurement.

III. THEORETICAL CALCULATIONS

In order to determine the most realistic doped structures, we performed structural relaxations on supercells of $(Na_{1-x}Li_x)_2IrO_3$ for Li dopings $0 \leqslant x \leqslant 1$ in steps of 0.125 within density functional theory (DFT). We considered the generalized gradient approximation (GGA) as the exchange-correlation functional and employed the projector augmented wave (PAW) basis set as implemented in the Vienna *ab initio* simulation package [8]. An $8 \times 6 \times 8$ k mesh was used. Since (i) the end compounds Na_2IrO_3 and Li_2IrO_3 show long range magnetic order and (ii) Ir is a 5d ion, magnetism, correlation, and spin-orbit coupling (SOC) effects may be important for precise structure predictions. However, DFT calculations including spin-orbit coupling are very time consuming. Therefore, we followed the following strategy. For the rather expensive determination of the most stable configurations for each doping level, we initially considered the GGA functional without inclusion of SOC and magnetism. The information gained from these results was subsequently used to perform more elaborate calculations including spin-orbit coupling, a Hubbard repulsion $U = 3$ eV, and spin polarization (spin-polarized GGA + SOC + U). We found that while these more precise calculations lead to much better comparison of lattice parameters with experiment, at the qualitative level the plain GGA calculations seem to be sufficient.

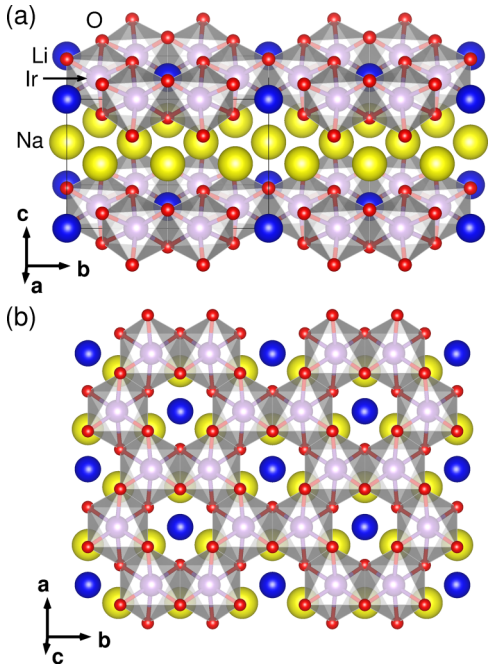

FIG. 1. (Color online) Calculated crystal structure of $(Na_{1-x}Li_x)_2IrO_3$ for $x = 0.25$: (a) Layered structure of Ir_2Li and Na_3 planes and (b) view on the Ir_2Li planes, where the Ir atoms form a honeycomb lattice.

For our GGA calculations we considered all possible Li configurations in a unit cell containing four formula units (f.u.) and searched for the most stable case. In order to verify the stability of the configurations, we also considered for some dopings supercells of sizes $2 \times 1 \times 1$ and $1 \times 2 \times 1$ where the unit cell with four formula units was doubled along a and along b, respectively. The total energy calculations obtained with the PAW basis were double checked against the all electron full potential local orbital (FPLO) code [9] (see Fig. 9 in Appendix B).

In our search for optimally relaxed structures, we considered two types of calculations. In one set of calculations the lattice parameters were fixed to the experimentally determined values [see Fig. 2(c)] and the internal coordinates were relaxed. In the second set of calculations we performed a full relaxation including both volume and internal coordinates. Both calculations showed that for $0 \leqslant x \leqslant 0.25$ the energetically most favorable location for Li ions are Na positions in the honeycomb layer. In Fig. 1 we present the most stable crystal structure of $(Na_{1-x}Li_x)_2IrO_3$ for a doping level of $x = 0.25$. For both types of relaxations (at fixed volume and including volume relaxation) the highest stability was obtained for Li substituting Na in the Ir_2Na planes rather than in the Na_3 planes. Further doping leads to a replacement of Na atoms in the Na_3 layer, where we found clustering of the Li atoms to be energetically favorable. This observation is also supported by the consideration of supercells containing eight formula units at a doping level of $x = 0.5$. In this case we found the structures with most clustering to be lowest in energy, while the configurations with a homogeneous distribution of Li atoms in the Na_3 layer are about 50 meV/f.u. (within GGA) higher in energy compared to the configurations with clustering.

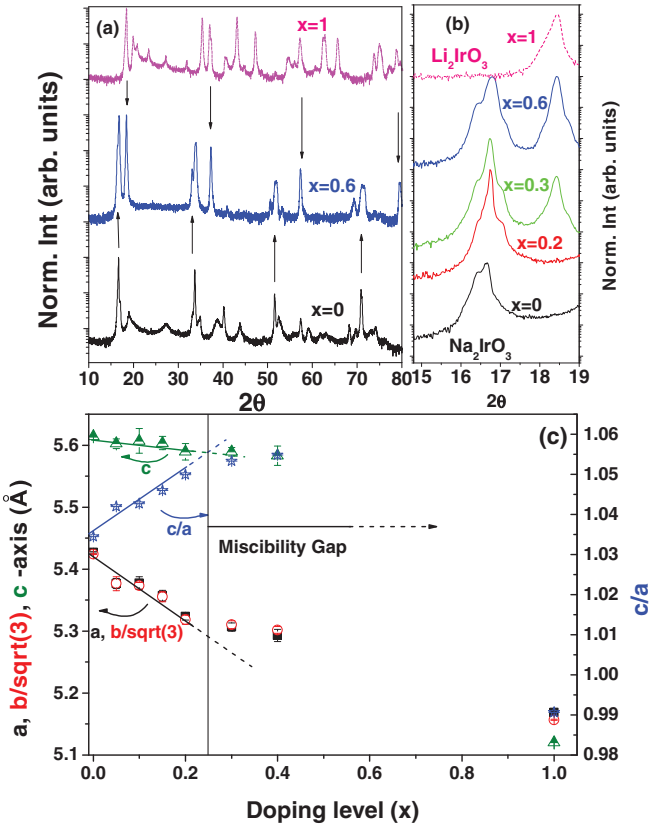

FIG. 2. (Color online) (a) Powder XRD of the crushed $(Na_{1-x}Li_x)_2IrO_3$ crystals for $x = 0,0.6$ and $x = 1$. The downward arrows point to $x = 0.6$ XRD peaks that match with $x = 1$ $(00n)$ peaks and upward arrows point to $x = 0.6$ XRD peaks that match with $x = 0$ $(00n)$ peaks. (b) Zoomed XRD spectra in the 2θ region 15°–19° for all values of x. (c) Lattice parameters obtained from single-crystal XRD of $(Na_{1-x}Li_x)_2IrO_3$ single crystals ($x = 1$ obtained from Ref. [10]). The horizontal arrow marks the miscibility gap region where samples showed phase separation. Solid straight lines (extended by dashed lines in the miscibility gap region) are guides to the eye.

IV. RESULTS AND DISCUSSION

A. Low doping ($x < 0.25$)

1. Structural changes

Powder XRD of crushed $(Na_{1-x}Li_x)_2IrO_3$ crystals shows single-phase crystals up to $x = 0.2$ [see Fig. 2(b)]. These crystals are very platelike and only $(00n)$ peaks could be observed. Moreover, while ICPMS confirms the inclusion of Li (see Table I) at the concentration $x = 0.2$, there is almost no shift of the (001) peak, implying almost no change in the c lattice parameter for the range $0 \leqslant x \leqslant 0.2$.

The lattice parameters as a function of doping were determined by single-crystal XRD. Complete diffraction patterns for structural refinement were collected for the best samples at each doping. Nevertheless we faced a few challenges when refining the diffraction pattern of the Li-doped samples. Namely, Li scatters x rays very weakly and its precise position in the structure cannot be uniquely determined from x-ray measurements alone, especially at low Li concentrations, and in the presence of dominant scatterers such as Ir (with 77 electrons), refinements of the crystal structure with Li in different Na positions (in the honeycomb Ir_2Na layer and in the hexagonal Na_3 layer) gave rather similar results. Since structural relaxation calculations (see the previous section) suggest a strong energetic preference for the doped Li to replace the Na in the Ir honeycomb layers (for $x \leqslant 0.25$), the final structural refinement (within SIR-92 and SHELX packages [11]) was performed assuming that Li randomly replaces Na at this site. The refinement converged well only when some finite degree of site mixing ($f > 0$) was assumed also on the nominally Ir honeycomb site, so that the occupation at this site was assumed to be $(1 - f)\mathrm{Ir} + f\mathrm{Na}$. In order to preserve the total atomic count, the honeycomb center site occupation was assumed to be $4x\mathrm{Li} + (1 - 4x - 2f)\mathrm{Na} + 2f\mathrm{Ir}$. The refined atomic positions are listed in Tables II–V for the doping concentrations $x = 0.05$–0.2 (see Appendix A).

In order to determine the lattice parameters accurately we measured for each doping between ten and 20 samples, and the obtained average values are plotted in Fig. 2(c), with the error bars indicating the spread of values for each nominal composition. Throughout the range $0.05 \leqslant x \leqslant 0.2$, the diffraction patterns show sharp peaks that could be well indexed and refined with a $C2/m$ crystal structure derived from the undoped ($x = 0$) parent Na_2IrO_3 in Ref. [2]. For lower dopings $x = 0.05,0.1$ we found samples where the diffraction patterns could be consistently indexed in terms of a single crystal (no twins). For dopings $x = 0.15,0.2$, samples showed two or three coexisting twins, and in this case refinement was successfully performed using multitwin techniques with the same unit cell parameters and crystal structure for all coexisting twins. Throughout the range $0.05 \leqslant x \leqslant 0.2$ the $C2/m$ crystal structure of parent Na_2IrO_3 provides a good description of the observed diffraction pattern, confirming single-phase crystals with this structure. Both the a and b lattice parameters strongly decrease at the same rate with increasing doping ($b/\sqrt{3} \simeq a$, which confirms a globally almost undistorted honeycomb Ir structure in the low Li-doped region) while the c parameter remains almost constant [Fig. 2(c)]. Remarkably, the c/a ratio increases with increasing doping x up to 0.2 [Fig. 2(c)] while it is reduced by 5% in fully doped ($x = 1$) Li_2IrO_3 compared to the undoped ($x = 0$) Na_2IrO_3. We conclude that there is no effective c-axis pressure in the low Li doping region.

In Fig. 3 we present the lattice parameters predicted by spin-polarized GGA + SOC + U calculations ($U = 3$ eV, $J = 0.5$ eV). In the range that was accessible experimentally, we find remarkably good agreement between the calculated lattice parameters and the experimental values, shown in Fig. 2(b). Although there exists a small overestimation in the whole range $0 \leqslant x \leqslant 0.25$, the trends are caught extremely well and we could even reproduce the increase in the c/a ratio obtained in the experiment.

2. Magnetic susceptibility

In Fig. 4 we show the temperature T dependence of the magnetic susceptibility $\chi(T) = M/H$ for $(Na_{1-x}Li_x)_2IrO_3$ for dopings $x = 0.05$–0.2 measured at $H = 1$ T between 2 and 300 K. The inverse susceptibility (χ^{-1}) (not shown) and susceptibility (χ) were fitted to the Curie-Weiss (CW) law $\chi(T) = \chi_0 + \frac{C}{T-\theta_W}$ (red lines in Fig. 4) between 150 and 300 K. For all x values measured, $\chi_0 \approx 10^{-4}$ cm^3/mol

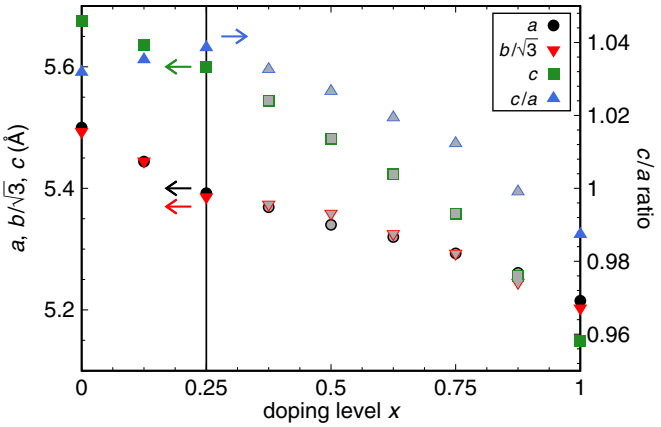

FIG. 3. (Color online) Calculated lattice parameters of $(Na_{1-x}Li_x)_2IrO_3$ within spin-polarized GGA + SOC + U. See the left axis for a, b, and c and the right axis for the c/a ratio. Lattice parameters for structures that, according to the total energy calculations plotted in Fig. 8, are only metastable are shown with gray symbols only.

and $C = 0.4$–0.5 cm^3 K/mol, while the Weiss temperature (θ_W) is dependent on doping [see Fig. 8(b)]. Since for single-crystalline Na_2IrO_3 an anisotropic susceptibility was observed [1], we expect a certain anisotropy in the different Li-substituted single crystals as well. The susceptibility measured on lumps of arbitrary oriented crystals is therefore different from the average between χ_a and χ_c and would not match a perfectly random polycrystalline sample. This explains a ≈20% variation in the C parameter of the Curie-Weiss fit for the different Li-substituted samples. $\chi(T)$ shows a kink for all measured x (marked with arrows in Fig. 4) indicating long range antiferromagnetic (AF) ordering. No spin-glass freezing has been observed, as confirmed by field-cooled (FC)–zero-field-cooled (ZFC) and ac susceptibility measurements. We determined the position of maxima by plotting $\frac{d\chi}{dT}$ vs T

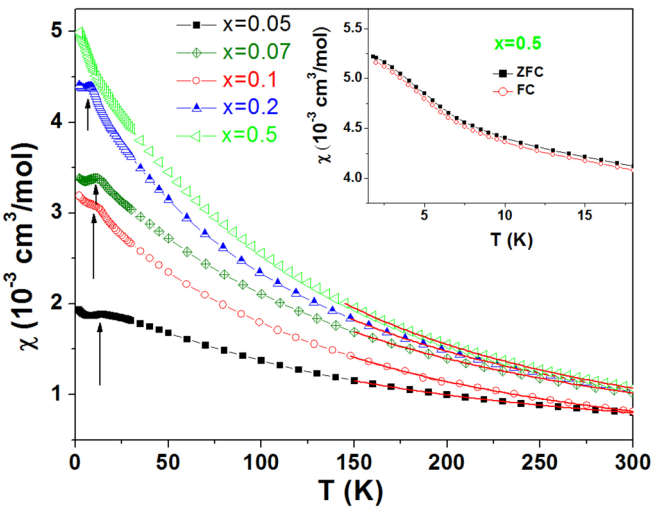

FIG. 4. (Color online) Magnetic susceptibility $\chi(T)$ vs T for $x = 0.05$–0.2 and $x = 0.5$. The red line indicates fitting by CW behavior $\chi = \chi_0 + \frac{C}{T-\theta_W}$. The arrows mark the positions of T_N. FC and ZFC measurements for $x = 0.5$ are shown in the inset.

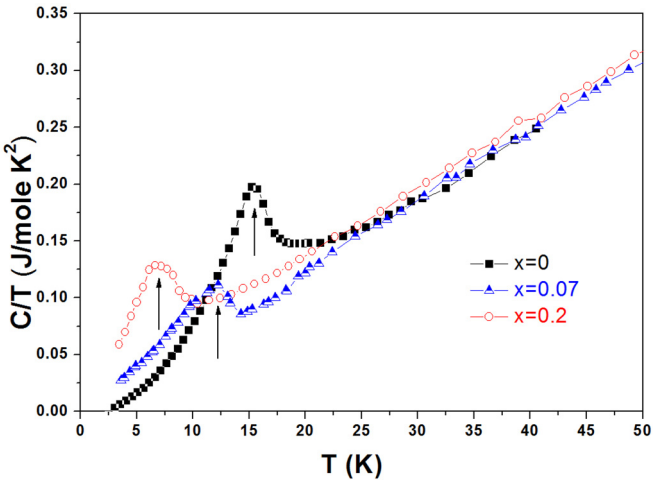

FIG. 5. (Color online) Heat capacity as $C(T)/T$ of single-phase $(Na_{1-x}Li_x)_2IrO_3$ crystals. The arrows mark the positions of T_N.

where the zero crossing is assigned to the AF transition temperature T_N.

3. *Heat capacity*

Figure 5 shows the heat capacity divided by the temperature (C/T) of $(Na_{1-x}Li_x)_2IrO_3$ crystals up to $x = 0.2$. These measurements confirm bulk AF ordering and the extracted T_N (from the onset of the lambdalike peaks in C/T) as a function of Li doping agrees with the values from the susceptibility measurements. In order to obtain information on the size of the ordered moment, we have determined the magnetic entropy from integration of the magnetic heat capacity [$\Delta C(T)/T$]. The latter was calculated by subtracting the phonon contribution. For $x = 0$ the phonon heat capacity is obtained from the nonmagnetic reference Na_2SnO_3 while for $x = 0.2$ we use as a reference a 80% contribution of Na_2SnO_3 and 20% of Li_2SnO_3. Integration of $\Delta C/T$ vs T reveals values of the magnetic entropy $\Delta S = 0.2R \ln 2$ and $0.12R \ln 2$ at T_N for $x = 0$ and 0.2, respectively. This suggests a suppression of the ordered moment ($0.22\mu_B$ at $x = 0$; see Ref. [12]) by Li substitution, which may be due to stronger frustration and/or local lattice distortions that affect the magnetic exchanges.

B. Higher doping ($x > 0.25$)

The systematic suppression of T_N with increasing x for $(Na_{1-x}Li_x)_2IrO_3$ crystals up to $x = 0.2$ suggests the possibility of a magnetic quantum phase transition at larger x. However, for larger Li content, i.e., from $x = 0.25$ to 0.6, we see a clear indication of phase separation in the respective samples. The powder XRD patterns of crushed crystals are shown in Figs. 2(a) and 2(b). Figure 2(a) shows that the $x = 0.6$ pattern contains ($00n$) peaks located close to both pure Li_2IrO_3 (marked by the downwards pointing arrows) and Na_2IrO_3 (indicated by the upwards pointing arrows). A closer inspection of the region near (001) with more different compositions is given in Fig. 2(b). It shows that, for all nominal compositions larger than 0.2, two phases are observed, one close to $x = 0.2$, and the other one $x = 1$. In the single-crystal XRD at the higher dopings $x = 0.3, 0.4$ the samples showed

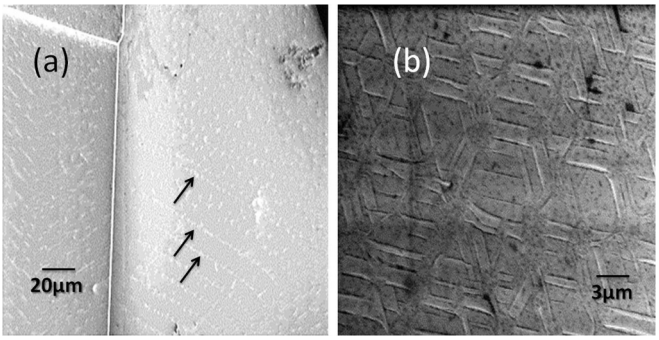

FIG. 6. SEM picture of (a) $x = 0.3$ and (b) $x = 0.6$ $(Na_{1-x}Li_x)_2IrO_3$ crystals.

many coexisting single-crystal grains compared to the crystals in the $x \leqslant 0.2$ doping region, and the diffraction data could not be consistently indexed by the same unit cell parameters for all coexisting grains, suggesting that the samples were not single phase, but possibly a mixture of phases with different lattice parameters.

The two phase scenario is further supported by the results of scanning electron microscopy (SEM) shown in Figs. 6(a) and 6(b) for $x = 0.3$ and 0.6 crystals, respectively. For $x = 0.3$ two phases were observed. On the lighter contrast lines [marked by arrows in Fig. 6(a)] EDX shows a much lower ratio of Na:Ir (almost only Ir). Hence this lighter contrast can be attributed to the Li_2IrO_3 phase. For $x = 0.6$ hexagonal shaped microdomains appear (average size 2–3 μm). The SEM picture was taken after cleaving the crystals, and microdomains of the same size are still present. EDX measurements show a very small Na:Ir ratio at the domain boundaries, indicating also Li_2IrO_3 microdomains. In fact, ICPMS indicates (Table I) an increase in Li content for $x \geqslant 0.3$, although there is not much change in the lattice parameters for $x = 0.3$ and 0.4 compared to $x = 0.2$ [see Fig. 2(c)]. The trend of change in lattice parameters significantly deviates after $x = 0.25$. This confirms that, in the region $0.25 < x \leqslant 0.6$, Li is not incorporated into the main $(Na_{1-x}Li_x)_2IrO_3$ phase, but rather forms separate microdomains of Li_2IrO_3, indicating a miscibility gap in the phase [see Fig. 8(b)].

This is further confirmed when heat capacity is measured for $0.25 \leqslant x \leqslant 0.6$. We observe in this whole range a smeared lambdalike peak at 5.5 K (Fig. 7), which implies that T_N does not depend on doping in this entire range. This means that the magnetic contribution originates from the main $Na_3Ir_2LiO_6$ phase, which is not affected by further doping. The microdomains of Li_2IrO_3 apparently do not exhibit long range order, presumably due to structural disorder [10]. For $x = 0.5$ magnetic susceptibility neither shows conventional antiferromagnetic (AF) ordering (Fig. 4) nor any separation between ZFC-FC susceptibility (inset), which is indicative of spin-glass behavior. We speculate that for this high doping region the presence of a multidomain Li_2IrO_3 phase smears out any AF transition in susceptibility.

Our DFT supercell calculations of $(Na_{1-x}Li_x)_2IrO_3$ at various dopings (see Sec. III) show that, in the $0 < x \leqslant 0.25$ range, $x = 0.125$ and 0.25 results are compatible with a uniform phase within the computational accuracy. However,

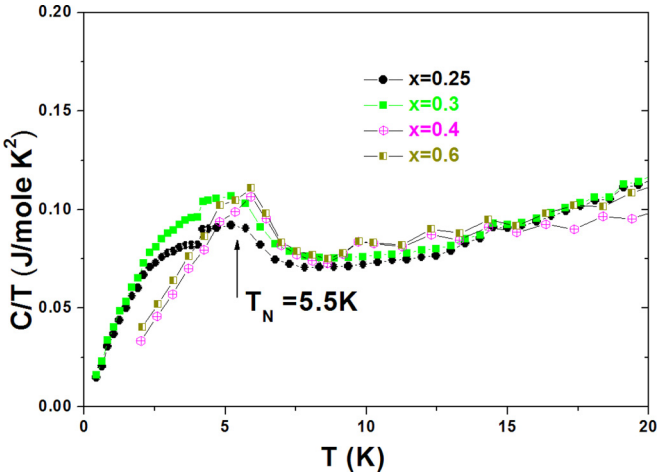

FIG. 7. (Color online) Heat capacity as $C(T)/T$ of multiphase $x \geqslant 0.25$. $(Na_{1-x}Li_x)_2IrO_3$ crystals. The arrows mark the positions of T_N which is fixed with increasing x.

after the Ir_2Na planes are completely substituted by Li, further doping ($x > 0.25$) is energetically unfavorable: For $0.25 < x < 1$ the energies of the lowest uniform phases are at least about 30 meV/Ir higher than those of the separated phases

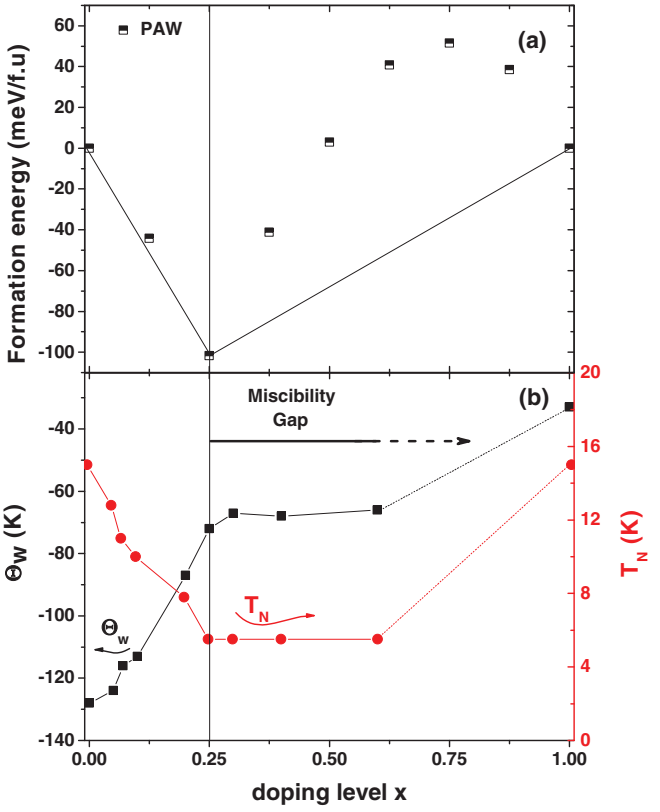

FIG. 8. (Color online) (a) Phase diagram of $(Na_{1-x}Li_x)_2IrO_3$ obtained from spin-polarized GGA + SOC + U total energy calculations. Shown are the formation energies obtained with the PAW basis. The vertical line indicates the composition at $x = 0.25$, which is a very stable $Na_3LiIr_2O_6$ structure with alternating $LiIr_2O_6$ and Na_3 layers. (b) Phase diagram with T_N and CW temperature θ_W of $(Na_{1-x}Li_x)_2IrO_3$, data at $x = 1$ are from Ref. [10]. The miscibility gap region is indicated by the horizontal arrow.

(see Fig. 9 in Appendix B). Moreover, the lowest-energy solutions tend to clusterize on the scale allowed by a given supercell. The inclusion of spin-orbit coupling, a Hubbard $U = 3$ eV, and magnetism [13] leads to an even more pronounced instability towards phase separation ($\gtrsim$40 meV/Ir), as shown in Fig. 8(a), where the straight line indicates the energy of the corresponding mixture of separated phases.

V. CONCLUSIONS

Based on our structural, thermodynamic, SEM, and magnetic measurements, as well as, first principles calculations, we propose the following scenario: In the $(Na_{1-x}Li_x)_2IrO_3$ system a miscibility gap emerges for $x > 0.25$ (Fig. 8). The stable structure in this region shows a phase separation into an ordered $Na_3Ir_2LiO_6$ phase, with alternating $LiIr_2O_6$ and Na_3 planes, and a Li-rich phase very close in composition to Li_2IrO_3. As the crystal grows, the $Na_3Ir_2LiO_6$ phase nucleates first, and forms the matrix. We suggest that nucleation for the Li_2IrO_3 phase should start at a higher temperature but at the low temperature it nucleates around multiple centers of the matrix $(Na_{1-x}Li_x)_2IrO_3$ phase, forming hexagonal microdomains.

However, one cannot completely exclude a possible high temperature solid-solution phase. One possibility could be that there may exist a critical temperature of the miscibility gap for each nominal composition $x \geqslant 0.25$ above which a metastable single phase exists, and that such a temperature is above the crystal growth temperature, and therefore it becomes extremely hard to get single-phase single crystals in this doping region. A recent work [5] has claimed single-phase crystals for $x = 0.7$–0.9. Our work reported here shows that in the doped samples we have synthesized, phase separation occurs for $0.25 \leqslant x \leqslant 0.6$ and very likely extends also for higher dopings, so a detailed investigation of the phase diagram for $0.25 < x < 1$, both stable and metastable, is highly desirable. In particular, such studies are needed to confirm the presence or absence of phase separation near $x = 0.7$, where earlier studies proposed that a continuous quantum phase transition occurs.

ACKNOWLEDGMENTS

We acknowledge Klaus Simon for ICPMS measurements, H. S. Jeevan for discussions on crystal growth and EDX analysis, and Yogesh Singh for collaboration. S.M. acknowledges funding from the Erasmus Mundus EURINDIA project. Work in Göttingen has been supported by the Helmholtz Virtual Institute 521 ("New states of matter and their excitations"). M.A., H.O.J., and R.V. acknowledge support by the Deutsche Forschungsgemeinschaft through Grant No. SFB/TR 49 as well as the Center for Scientific Computing (CSC) in Frankfurt. Work at Oxford has been supported by EPSRC (U.K.). I.I.M. acknowledges Funding from the Office of Naval Research (ONR) through the Naval Research Laboratory's Basic Research Program, and support from the A. von Humboldt foundation.

TABLE II. Structural parameters for $x = 0.05$ Li doping from single-crystal x-ray data at 300 K. [$C2/m$ space group, $a = 5.379(5)$ Å, $b = 9.314(5)$ Å, $c = 5.594(5)$ Å, $\beta = 108.714(5)^\circ$, $Z = 4$.] U is the isotropic displacement. The goodness of fit (S) was 1.269, $w_{R_2} = 0.1684$, $R_1 = 0.0632$ ($R_{\rm int} = 0.0797$, $R_\sigma = 0.051$).

Atom	Site	x	y	z	Occ	U (Å^2)
Ir1	4g	0.5	0.1667(1)	0	0.849	0.0074(6)
Na1	4g	0.5	0.1667(1)	0	0.151	0.0074(6)
Na2	2a	0	0	0	0.498	0.0092(8)
Ir2	2a	0	0	0	0.302	0.0092(8)
Li2	2a	0	0	0	0.2	0.0092(8)
Na3	2d	0.5	0	0.5	1	0.021(4)
Na4	4h	0.5	0.3384(9)	0.5	1	0.019(3)
O1	8j	0.758(3)	0.1732(11)	0.792(3)	1	0.013(3)
O2	4i	0.720(4)	0	0.210(4)	1	0.013(4)

TABLE III. Same as Table II for $x = 0.10$. $S = 1.467$, $w_{R_2} = 0.2143$, and $R_1 = 0.0753$ ($R_{\rm int} = 0.053$, $R_\sigma = 0.0515$).

Atom	Site	x	y	z	Occ	U (Å^2)
Ir1	4g	0.5	0.1668(1)	0	0.8303	0.0065(4)
Na1	4g	0.5	0.1668(1)	0	0.1697	0.0065(4)
Na2	2a	0	0	0	0.2605	0.0171(7)
Ir2	2a	0	0	0	0.3395	0.0171(7)
Li2	2a	0	0	0	0.4	0.0171(7)
Na3	2d	0.5	0	0.5	1	0.022(3)
Na4	4h	0.5	0.3384(7)	0.5	1	0.023(3)
O1	8j	0.757(2)	0.1734(8)	0.791(2)	1	0.014(3)
O2	4i	0.719(3)	0	0.213(3)	1	0.013(3)

APPENDIX A: SINGLE-CRYSTAL X-RAY REFINEMENT RESULTS

In Tables II–V we list the structures of $(Na_{1-x}Li_x)_2IrO_3$ in the doping range $x = 0.05$–0.20 as determined by x-ray diffraction.

APPENDIX B: PHASE DIAGRAM OBTAINED FROM GGA CALCULATIONS

Figure 9 shows the formation energy of the $(Na_{1-x}Li_x)_2IrO_3$ structures predicted within GGA. The calculations were done with VASP (PAW basis) [8] and with an all electron code (FPLO) [9]. Qualitatively, the formation energy is very

TABLE IV. Same as Table II for $x = 0.15$. The sample had two twins rotated around the c^* axis with $R_{\rm int} = 0.168$ and 0.198 for the data sets of reflections for grain 1 (similar parameters for grain 2), with the combined goodness-of-fit values $S = 1.778$, $w_{R_2} = 0.2679$, and $R_1 = 0.1151$.

Atom	Site	x	y	z	Occ	U (Å^2)
Ir1	4g	0.5	0.1669(2)	0	0.915	0.009(1)
Na1	4g	0.5	0.1669(2)	0	0.085	0.009(1)
Na2	2a	0	0	0	0.23	0.019(3)
Ir2	2a	0	0	0	0.17	0.019(3)
Li2	2a	0	0	0	0.6	0.019(3)
Na3	2d	0.5	0	0.5	1	0.025(6)
Na4	4h	0.5	0.3394(16)	0.5	1	0.022(4)
O1	8j	0.756(4)	0.177(2)	0.792(4)	1	0.016(5)
O2	4i	0.709(5)	0	0.204(5)	1	0.005(5)

TABLE V. Same as Table II for $x = 0.20$. The sample had three twins rotated around the c^* axis with the R_{int} parameter between 0.15 and 0.30 for the three data sets of reflections, with the combined goodness-of-fit values $S = 2.091$, $w_{R_2} = 0.3019$, $R_1 = 0.1237$.

Atom	Site	x	y	z	Occ	U (Å^2)
Ir1	4g	0.5	0.1671(1)	0	0.9038	0.011(1)
Na1	4g	0.5	0.1671(1)	0	0.0962	0.011(1)
Na2	2a	0	0	0	0.0075	0.015(2)
Ir2	2a	0	0	0	0.1925	0.015(2)
Li2	2a	0	0	0	0.8	0.015(2)
Na3	2d	0.5	0	0.5	1	0.027(5)
Na4	4h	0.5	0.3377(14)	0.5	1	0.030(4)
O1	8j	0.759(5)	0.1780(17)	0.805(5)	1	0.025(5)
O2	4i	0.716(5)	0	0.191(5)	1	0.019(5)

similar to the computationally more expensive spin-polarized GGA + SOC + U results (compare Fig. 8).

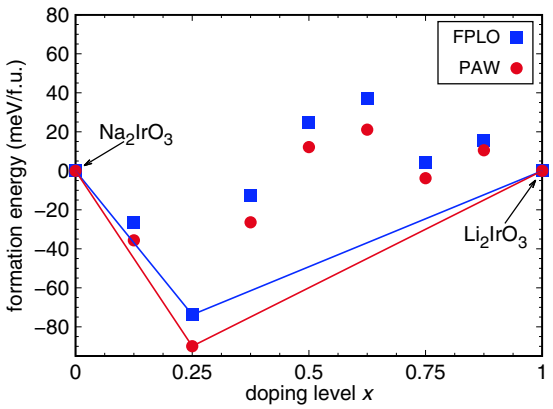

FIG. 9. (Color online) Formation energies of $(Na_{1-x}Li_x)_2IrO_3$ obtained from DFT total energy calculations within GGA indicate a stable composition range $0 \leqslant x \leqslant 0.25$ and a tendency to phase separate for $0.25 < x < 1$, in agreement with the GGA+SO+U result (Fig. 8).

[1] Y. Singh and P. Gegenwart, Phys. Rev. B **82**, 064412 (2010).

[2] S. K. Choi, R. Coldea, A. N. Kolmogorov, T. Lancaster, I. I. Mazin, S. J. Blundell, P. G. Radaelli, Y. Singh, P. Gegenwart, K. R. Choi, S.-W. Cheong, P. J. Baker, C. Stock, and J. Taylor, Phys. Rev. Lett. **108**, 127204 (2012).

[3] A. Shitade, H. Katsura, J. Kuneš, X.-L. Qi, S.-C. Zhang, and N. Nagaosa, Phys. Rev. Lett. **102**, 256403 (2009).

[4] J. Chaloupka, G. Jackeli, and G. Khaliullin, Phys. Rev. Lett. **105**, 027204 (2010).

[5] G. Cao, T. F. Qi, L. Li, J. Terzic, V. S. Cao, S. J. Yuan, M. Tovar, G. Murthy, and R. K. Kaul, Phys. Rev. B **88**, 220414(R) (2013).

[6] I. I. Mazin, H. O. Jeschke, K. Foyevtsova, R. Valentí, and D. I. Khomskii, Phys. Rev. Lett. **109**, 197201 (2012).

[7] K. Foyevtsova, H. O. Jeschke, I. I. Mazin, D. I. Khomskii, and R. Valentí, Phys. Rev. B **88**, 035107 (2013).

[8] G. Kresse and J. Hafner, Phys. Rev. B **47**, 558 (1993).

[9] K. Koepernik and H. Eschrig, Phys. Rev. B **59**, 1743 (1999).

[10] Y. Singh, S. Manni, J. Reuther, T. Berlijn, R. Thomale, W. Ku, S. Trebst, and P. Gegenwart, Phys. Rev. Lett. **108**, 127203 (2012).

[11] A. Altomare, G. Cascarano, C. Giacovazzo, and A. Guagliardi, J. Appl. Crystallogr. **27**, 435 (1994); G. M. Sheldrick, Acta Crystallogr. A **64**, 112 (2008).

[12] F. Ye, S. Chi, H. Cao, B. C. Chakoumakos, J. A. Fernandez-Baca, R. Custelcean, T. F. Qi, O. B. Korneta, and G. Cao, Phys. Rev. B **85**, 180403(R) (2012).

[13] The structural relaxations under inclusion of SOC and magnetism (stabilized by the use of an on-site Hubbard repulsion of reasonable strength, $U = 3$ eV) were performed for the most stable configurations as obtained in the relaxations described in Sec. III.